JOURNAL OF AERONAUTICS AND SPACE TECHNOLOGIES
(ISSN: 1304-0448)
July 2021 Volume 14 Number 2
jast.hezarfen.msu.edu.tr

Research Article

Structural Behavior Examination of Frequently Used Solid Propellant Sections Under Centrifugal Loading Using Response Surface Method

Ceyhun TOLA[1*], Hatice Begüm EYLENOĞLU[2]

[1] *Aselsan Inc., Microelectronics, Guidance & Electro-Optics Division, 06750 Ankara, Turkey*, ctola@aselsan.com.tr, https://orcid.org/0000-0001-9056-0543

[2] *University of Turkish Aeronautical Association, Department of Astronautical Engineering, 06790 Ankara, Turkey*, haticebegumeylenoglu@gmail.com, https://orcid.org/0000-0001-5619-3620

* *Corresponding Author*

Article Info

Received: *April 23, 2021*
Accepted: *July 6, 2021*
Online: *July 26, 2021*

Keywords: Solid Rocket Motor, Centrifugal Loading, Finite Element Analysis, Viscoelasticity, Response Surface Method

Abstract

This research aims to examine structural responses of frequently used solid propellant sections such as tubular, star, slotted, wagon wheel, and anchor subjected to centrifugal acceleration load. Viscoelastic finite element models of the grains having different dimensions are constructed and solved in the Abaqus environment using in-house parametric Python scripts prepared within the content of this work. Validation of the finite element models is accomplished by comparing finite element results with an analytical equation found in the literature. Finally, different response surfaces are constructed in the Minitab environment to determine the effect of grain cross-section parameters on von Mises stress level of the propellant. Thus, the most effective cross-section parameters on von Mises stress are determined for the examined grain shapes.

To Cite This Article: Ceyhun TOLA, Hatice Begüm EYLENOĞLU "Structural Behavior Examination of Frequently Used Solid Propellant Sections Under Centrifugal Loading Using Response Surface Method", Journal of Aeronautics and Space Technologies, Vol. 14, No. 2, pp. 231-242, July. 2021.

Sık Kullanılan Katı Yakıt Geometrilerinin Dönme Yükü Altındaki Yapısal Davranışının Cevap Yüzeyi Yöntemi Kullanılarak İncelenmesi

Makale Bilgisi

Geliş: *23 Nisan 2021*
Kabul: *6* Temmuz *2021*
Yayın: *26 Temmuz 2021*

Anahtar Kelimeler: Katı Yakıtlı Roket Motoru, Dönme Yükü, Sonlu Elemanlar Yöntemi, Viskoelastisite, Cevap Yüzeyi Yöntemi

Öz

Bu çalışma, dairesel, yıldız, oluklu, vagon tekeri ve çapa gibi kesitlere sahip katı yakıt geometrilerinin dönme yükü (merkezkaç kuvveti) altındaki yapısal cevaplarını incelemeyi amaçlamaktadır. Farklı kesit boyutlarına sahip viskoelastik katı yakıt modellerinin sonlu elemanlar analizleri, çalışma kapsamında hazırlanan parametrik Python kodları kullanılarak Abaqus ortamında gerçekleştirilmiştir. Sonlu elemanlar modelleme tekniğinin doğrulaması, literatürden temin edilen bir analitik eşitlik yardımıyla tamamlanmıştır. Son olarak, katı yakıtlara ait kesit parametrelerinin von Mises gerilme seviyesi üzerine olan etkilerini ortaya çıkartmak amacıyla Minitab ortamında farklı cevap yüzeyleri oluşturulmuştur. Böylece, incelenen yakıt geometrileri için von Mises gerilmesi üzerinde en yüksek etkiye sahip kesit parametreleri belirlenmiştir.

1. INTRODUCTION

Solid rocket motor technology has a wide usage area covering both civil and military purposes. Giant solid booster motors are designed and used for spacecraft launch applications while smaller versions are preferred for military purposes. Depending on the application, different performance requirements should be satisfied by generally changing the grain's cross-section in order to provide a suitable thrust time curve. On the other hand, the grain should preserve its structural integrity under different loading conditions, such as cool-down, ignition, centrifugal and longitudinal accelerations, etc. Therefore, in literature, some of the studies focus on the examination of the internal ballistic performance of solid rocket motors while some of them focus on structural integrity under different loading conditions. This research only focuses on the structural integrity of solid propellants. Thus, the internal ballistic performance issue is out of the scope of this work; so, the literature review covers only the structural integrity issue.

Shen et al. performed structural integrity analysis of a solid rocket motor grain under the cool-down and ignition pressure combined loading condition [1]. Gligorijević et al. carried out a structural analysis of a 122 mm rocket propellant grain under thermal and acceleration loads [2]. Qu and Zhang performed structural analysis of a solid rocket motor under acceleration loads during ship motion [3]. Chu and Chou examined the effect of cooling rate on solid

propellant's safety factor [4]. Adel and Guozhu studied modeling bore deformation of a tubular grain under cool-down loading and compared their results with experimental results determined within the context of their work [5]. Kurian et al. carried out structural analysis of tubular grain under storage and pressure loads [6]. Tunç and Özüpek performed thermal cyclic stress analysis of a three-dimensional solid rocket motor model to provide information about its life assessment [7].

During a solid rocket motor development process, combined load case scenario covering all of the different loading conditions (cool-down, ignition, centrifugal and longitudinal accelerations) should be examined carefully. However, analysis of different grains under combined load does not provide generalized results about which grain variable is much more critical on which type of loading.

Effects of cool-down, ignition, and longitudinal acceleration loads and storage are examined in different works so far. On the other hand, effects of centrifugal loading (rotational body force) on the structural integrity of frequently used grain sections such as tubular, star, slotted, wagon wheel, anchor, etc. are not examined in the literature. However, the structural endurance of a grain section under centrifugal loading is critical since some of the munitions are ejected with spinning from their launchers in order to increase their stability.

Within the content of this work, the response surface method is used to perform the structural behavior examination of the grain configurations exposed to centrifugal loading in order to determine which grain variable is much more critical for different grain geometries on the maximum stress level governing from the rotational body force. First of all, the linear viscoelastic finite element model is validated using analytical solutions of simple geometry. Then, parametric Python scripts are prepared for each grain type in order to construct and solve finite element models quickly. Finally, response surfaces are produced and validated after accomplishing required finite element analyses for surface construction. Parametric finite element models are prepared in the Abaqus environment and response surface analyses are conducted in Minitab software. As a result, the effects of different cross-section parameters on von Mises stress level on the frequently used grain geometries are examined.

2. FINITE ELEMENT MODEL

This section covers the properties of finite element models prepared for the grain configurations that are used for response surface construction.

2.1. Solid Rocket Motor Geometry

A basic solid rocket motor consists of a motor case, insulation, propellant, nozzle, and igniter as can be seen from Figure 1.

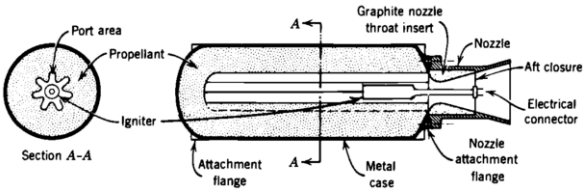

Figure 1. Solid rocket motor components [8].

Motor case (metal case) covers propellant, insulation, igniter inside it and endures various loading conditions during ignition and flight. Generally, insulation is located between the motor case and the propellant to isolate the motor case against high combustion temperature. Solid propellant stores energy needed during ignition and flight. Igniter initiates the launch process and the nozzle accelerates burned gasses through it.

Different grain configurations can be preferred depending on mission's thrust – time requirements considering their structural strength. Grains having tubular, star, slotted, wagon wheel, and anchor cross-sections are frequently preferred for different applications. Figure 2 illustrates the cross-sections.

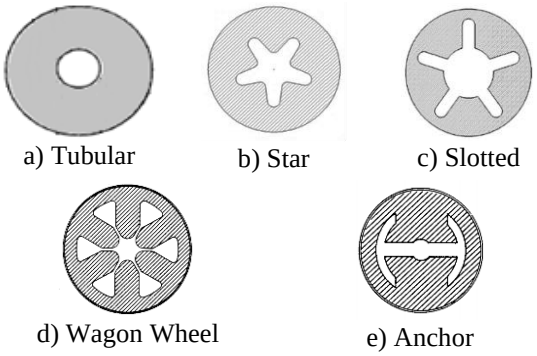

Figure 2. Frequently used grain geometries [9-10].

A few cross-section parameters are enough to define them. Figure 3 to 7 defines and illustrates those parameters for each of them. Parameter N defines the numbers of slots for the star, slotted, wagon wheel, and anchor geometries.

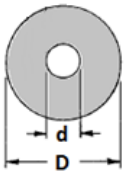

Figure 3. Cross-section parameters of tubular grains adapted from [9].

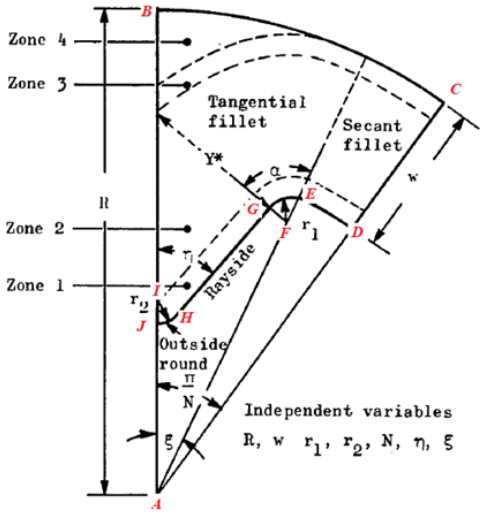

Figure 4. Cross-section parameters of star grains adopted from [9].

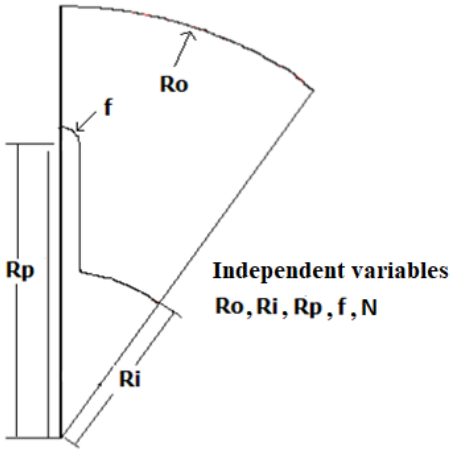

Figure 5. Cross-section parameters of slotted grains adopted from [11].

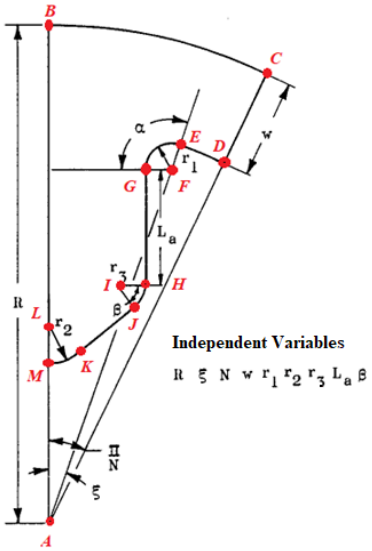

Figure 6. Cross-section parameters of wagon wheel grains adopted from [9].

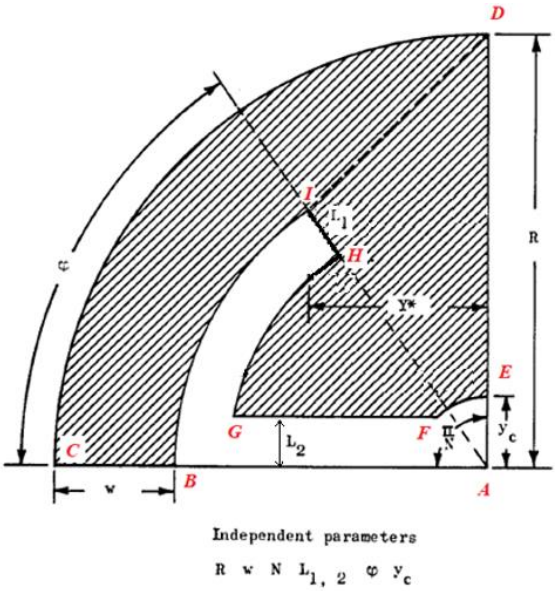

Figure 7. Cross-section parameters of anchor grains adopted from [9].

In order to prepare and solve a lot of finite element models which are required to construct response surfaces as soon as possible with high accuracy; the plane strain modeling technique having symmetry boundary conditions is preferred assuming that the cross-section of solid rocket motors is constant.

2.2. Material Properties

It is assumed that the motor case is produced from Maraging 250 steel, ethylene propylene diene monomer (EPDM) based insulation material, and hydroxyl-terminated polybutadiene (HTPB) based solid propellant is used for the solid rocket motor.

The propellant is modeled using a linear viscoelastic model considering its material properties. In order to define its stiffness with respect to temperature and time, Prony series stated in (1) and Williams-Landel-Ferry (WLF) function given in (2) are used [12].

$$E(t) = E_\infty + \sum_{i=1}^{n} E_i \cdot \exp\left(\frac{-t}{\lambda_i}\right) \quad (1)$$

where, E_∞ is long-term relaxation modulus, and E_i corresponds to relaxation modulus constants. Time is symbolized with t and λ_i is named as time constants.

$$log(a_t) = \frac{-C_1(T - T_0)}{C_2 + (T - T_0)} \quad (2)$$

where, C_1 and C_2 are named as WLF coefficients. T is instantaneous temperature and T_0 corresponds to reference temperature.

Mechanical properties of the materials are listed Table 1. Prony Series coefficients and WLF coefficients are tabulated in Table 2 and 3 respectively. The master curve of the propellant is given in Figure 8.

Table 1. Mechanical properties of materials [10].

Properties	Maraging 250 Steel	EPDM based Insulation	HTPB based propellant
E, MPa	190000	500	1.09 (E_∞)
ν	0.3	0.3	0.499
ρ, kg/m^3	8000	1000	1700

Table 2. Prony series coefficients of propellant [10].

i	E_i	λ_i
1	7.664	0.0007
2	7.844	0.0052
3	3.600	0.0578
4	2.536	0.4059
5	1.390	3.5383
6	0.816	37.6457
7	0.757	240.954
8	0.041	3030.30
9	0.429	6905.38
10	0.619	191.149

Table 3. WLF function coefficients of propellant [10].

C_1	C_2	T, °C
210.2	4542.4	35

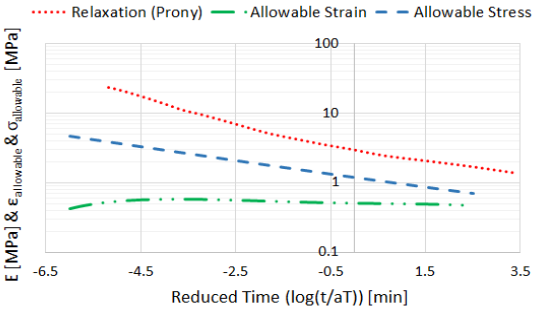

Figure 8. Master curve of the propellant [10].

It should be noted that the propellant used in this study is generic so its properties do not belong to a real one. On the other hand, the defined properties imitate real propellant behavior as it is supposed to be. Figure 9 illustrates material distribution on a sample wagon wheel grain configuration.

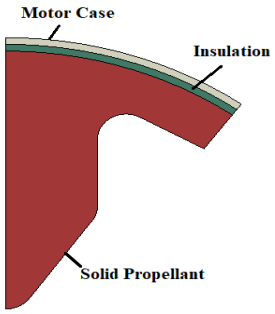

Figure 9. Material distribution on a sample cross-section.

Similar material distributions are also applied for all other finite element models.

2.3. Loads and Boundary Conditions

Symmetry boundary conditions are applied to all finite element models to lessen the solution time without sacrificing accuracy. Centrifugal acceleration force is applied as a rotational body force. It is assumed that 500 rpm (52.36 rad/s) rotational body force is exerted on the models in 1 second.

Figure 10 illustrates the loads and boundary conditions of the sample wagon wheel grain configuration.

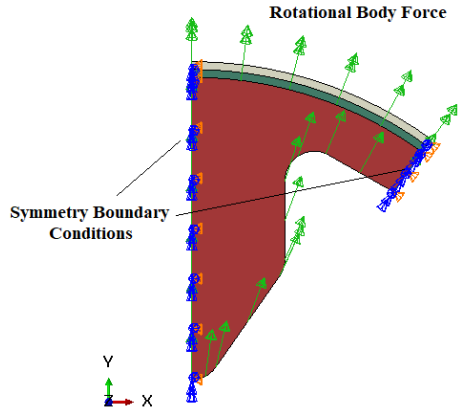

Figure 10. Loads and boundary conditions on a sample cross-section.

A similar modeling strategy is also applied to all other finite element models.

2.4. Mesh Structure

Quadrilateral plane strain elements having 1 mm approximate edge size are used for all models. Motor case and insulation are modeled with CPE8 8 node biquadratic plane strain elements having full integration while solid propellants are modeled with CPE8RH 8 node biquadratic plane strain elements having reduced integration and hybrid formulation. Reduced integration leads to higher strain values on the propellant and this is conservative in terms of strain since propellants are generally failed due to high strain value. The hybrid formulation is also preferred considering the propellant's high Poisson ratio value.

Sample mesh structures belonging to different grain configuration samples are presented in Figure 11.

2.5. Model Parametrization

During the construction of the response surfaces, a lot of models have to be prepared and solved. In order to accomplish this process in less amount of time without causing any human error; parametric Python scripts which can easily construct and solve the finite element models of the different grain configurations are prepared.

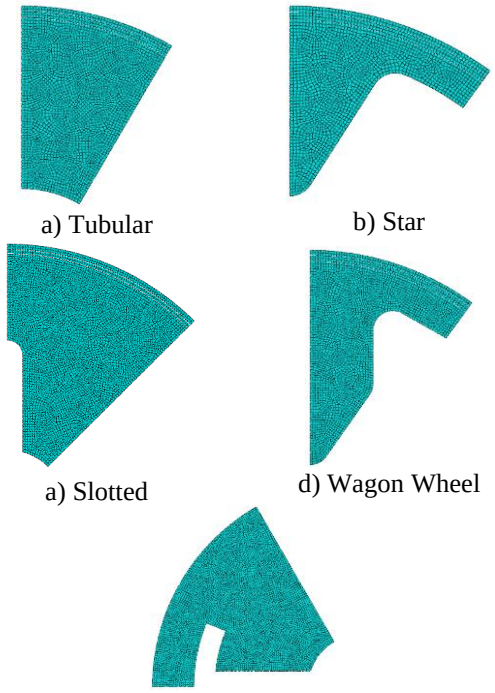

Figure 11. Sample mesh structures for each grain type.

3. VALIDATION

Before performing finite element solutions, to be sure that the modeling technique is correct, a validation study is conducted.

Radial stress at the most outer surface of a tubular grain (Figure 12) subjected to centrifugal loading can be determined using (3) [13].

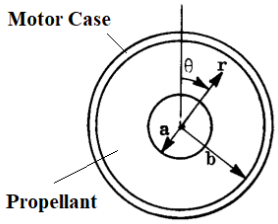

Figure 12. Tubular grain geometry used for validation [13].

$$\sigma_{rr}(b) = \frac{-\left[\frac{\left(\left(\frac{b}{a}\right)^2-1\right)\omega^2}{6}\right]\left[3a^2\frac{\rho_p}{g}-\left(4b^2\frac{\rho_c}{g}(1-\nu_c{}^2)\frac{E_p}{E_c}\right)\right]}{1+\frac{2}{3}\left[\left(\frac{b}{a}\right)^2-1\right](1-\nu_c{}^2)\frac{b\cdot E_p}{h\cdot E_c}} \quad (3)$$

where, a and b are inner and outer radius of the propellant respectively. Motor case thickness is defined by h. E_p and E_c defines modulus of elasticity corresponding to the propellant and the motor case; ρ_p and ρ_c are propellant and motor case densities respectively. Poisson's ratio of the motor case is defined by ν_c, gravitational acceleration corresponds to g and spin rate is defined by ω.

It is assumed that ω=50 rad/s spin rate is exerted on the tubular grain in 1 second. Instantaneous stiffness of the propellant is calculated benefiting from the Prony series previously stated in (1) and using the properties listed in Tables 1 and 2.

Table 4 summarize material properties and Table 5 lists geometric dimensions of the motor used in the validation process. The gravitational acceleration value is taken as 9.80665 m/s^2.

Table 4. Material properties used in validation.

Properties	Motor Case	Propellant
E, MPa	190000	4.994 (for t=1s)
ν	0.3	Not used
ρ, kg/m^3	8000	1800

Table 5. Dimensions of the tubular grain used in the validation case.

a	100 mm
b	300 mm
h	10 mm

The loading scenario is also modeled and solved in the Abaqus environment using the same modeling technique expressed in Section 2. Finite element analysis results covering radial stress components of the propellant are shown in Figure 13.

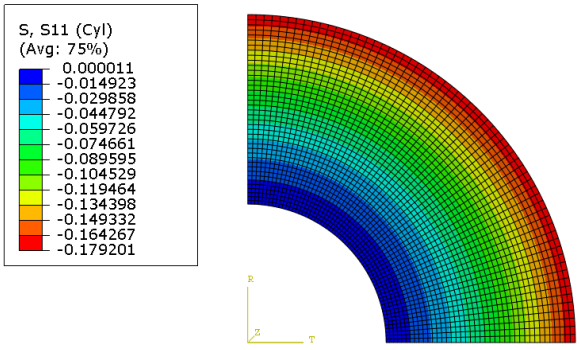

Figure 13. Finite element analysis results of the validation case, radial stress distribution (MPa).

Comparison of the finite element analysis and analytical results for the most outer region of the propellant can be seen in Table 6.

Table 6. Comparison of analytical and finite element results.

Properties	Analytical Results	Finite Element Results	Error (%)
$\sigma_{rr}(b)$, kPa	-179.085	-179.201	0.065

According to Table 6, finite element results are in good agreement with the analytical results. Thus, the modeling technique explained in Section 2 can be used.

4. STRUCTURAL ANALYSIS RESULTS

This section covers the finite element analysis results of the solid propellant sections under centrifugal loading. For each case, the outer radius of the propellant is kept constant (R = 100 mm). Critical locations in terms of von Mises stress are determined and illustrated for each grain type.

4.1. Tubular Grain

Tubular grain has 2 independent cross-section parameters those are inner and outer radius. Finite element analysis results show that maximum von Mises stress occurs at the inner bore of the propellant up to a certain inner radius limit (Figure 14) and further increment of inner radius leads to a decrement of maximum von Mises stress level on it. After a certain inner radius threshold, further increment of the inner radius shifts maximum stress location to the most outer surface of the propellant (Figure 15) since its propellant volumetric loading fraction is low enough.

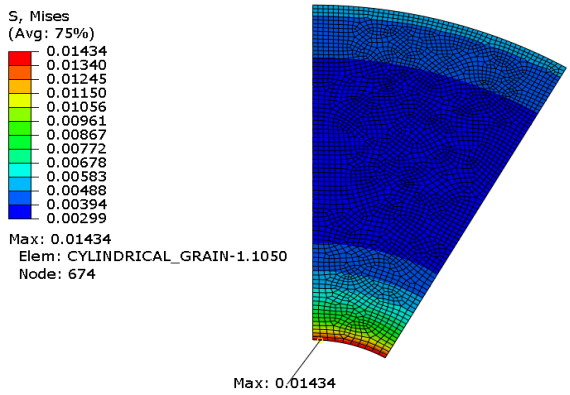

Figure 14. Sample finite element analysis result of tubular grain (for high volumetric loading fraction, r_i=20 mm) (MPa).

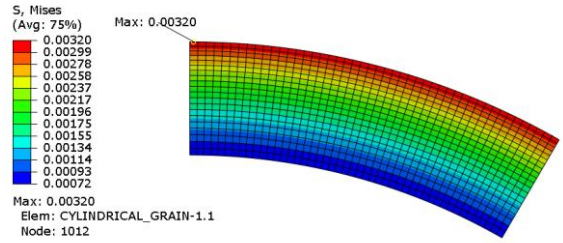

Figure 15. Sample finite element analysis result of tubular grain (for low volumetric loading fraction, r_i=80 mm) (MPa).

4.2. Star Grain

Star grain has 7 independent cross-section parameters which are illustrated in Figure 4. According to the results, maximum von Mises stress occurs at the slot radius of the star grain (Figure 16).

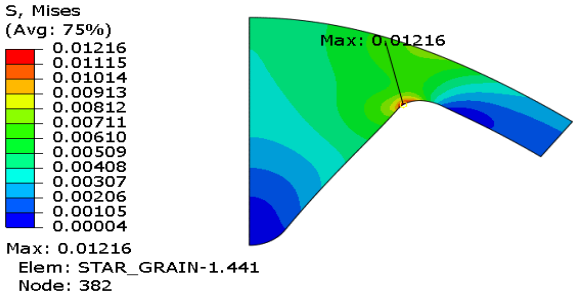

Figure 16. Sample finite element analysis result of star grain (MPa).

4.3. Slotted Grain

Slotted grain has 5 independent cross-section parameters which are illustrated in Figure 5. Similarly, maximum von Mises stress occurs at the slot radius of the propellant (Figure 17).

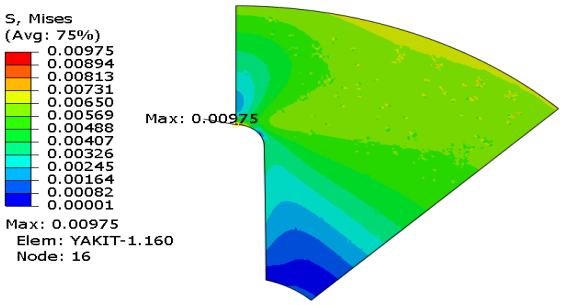

Figure 17. Sample finite element analysis result of slotted grain (MPa).

4.4. Wagon Wheel Grain

Wagon grain has 9 independent cross-section parameters which are illustrated in Figure 6. Finite element analysis results show that maximum von Mises stress occurs at the upper radius of the wagon wheel grain (Figure 18).

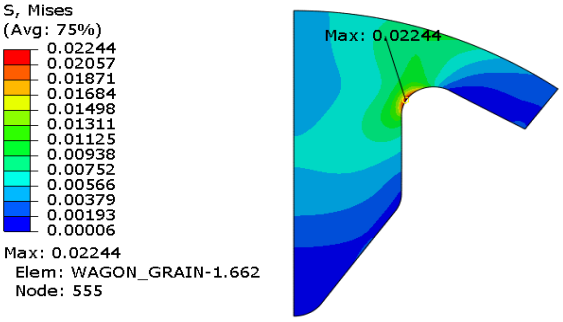

Figure 18. Sample finite element analysis result of wagon wheel grain (MPa).

4.5. Anchor Grain

Anchor grain has 7 independent cross-section parameters those are listed in Figure 7. According to the

results, maximum von Mises stress occurs at the anchor-shaped slot's upper corner (Figure 19).

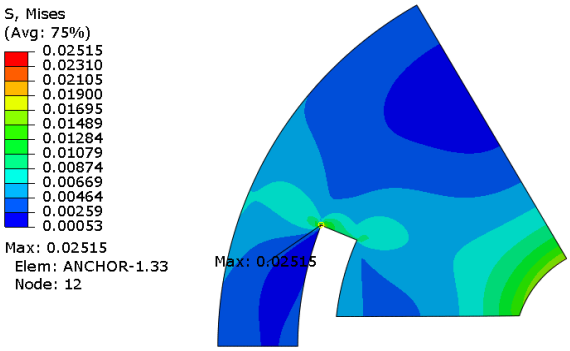

Figure 19. Sample finite element analysis result of anchor grain (MPa).

5. RESPONSE SURFACE RESULTS

Response surface analysis is used to determine the response of an output parameter (response) to input variables (response variables). Different methods such as Central Composite or Box-Behnken can be applied for response surface design. The Face-Centered Central Composite Design method is preferred for the response surfaces constructed within the content of this work.

Response surface is a mathematical model and if the correlation between experimental data (real data) and the data derived from the response surface (mathematical data) are good enough; it is possible to make fast and accurate calculations inside the boundaries of the response variables. On the other hand, it is not reliable to use response surface results if response surface variables are out of the boundaries and so extrapolation is needed.

Usage of the response surface method provides valuable information to designers. For example, response surfaces clarify that whether there is a linear or nonlinear relationship between the output and the input variables. This method also easily reveals the most effective parameter on the response. In the light of the response surface analysis results, it is possible to conduct a very quick virtual optimization study by solely using a mathematical model to significantly lessen the optimization process. On the other hand, the results of the virtual optimization studies have to be checked by performing a final real analysis to be sure about its accuracy.

This section covers response surface analysis results of different grain types subjected to centrifugal loading. Cross-section parameters except for constant outer radius (R = 100 mm) are defined as response variables (inputs) while maximum von Mises stress on the propellant due to the rotational body force is defined as the response (output).

5.1. Tubular Grain

Tubular grain has only two cross-section parameters and since one of them (outer radius) is constant (100 mm), it is not possible to construct a response surface with only one variable (inner radius). Instead, basic regression analysis in MS Excel can be accomplished by performing 17 different finite element analyses and using results of them as real data set. The number of analyses (17) is selected arbitrarily so less amount of analyses is also enough to illustrate the behavior of the maximum stress variation. Figure 20 represents the variation of maximum von Mises stress level on the propellant with the variation of inner radius. Boundaries of the inner radius (port radius) are presented in Table 7.

Table 7. Response variables and boundaries for tubular grain.

Variable	Min.	Max.
r_i, mm	20	80

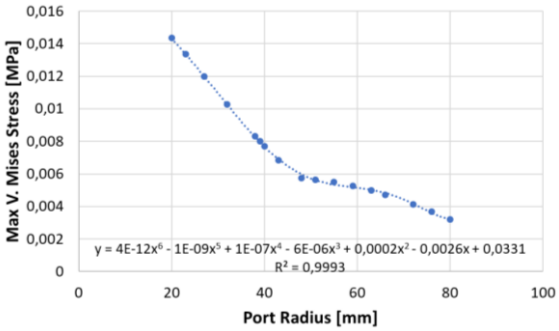

Figure 20. Variation of von Mises stress with inner radius for tubular grain.

An increment of the inner radius leads to a decrement of maximum von Mises stress level on the propellant.

A smaller inner radius means higher propellant volume and so higher propellant fraction ratio. Whenever the inner radius is smaller than a certain threshold (for this example r = 48 mm) maximum von Misses stress is located at the inner bore of the radius.

If the inner radius is bigger than the threshold, the stress level at the inner bore is decreased and the maximum von Mises stress is shifted to the most outer surface of the propellant. When the maximum stress location is shifted to the outer surface, further increment of the inner radius is less effective on maximum von Mises stress level when it is compared with the previous case. Therefore, the slope of the curve's left-hand side illustrated in Figure 20 is higher than its right-hand side.

5.2. Star Grain

To construct the response surface, 77 different finite element models having different dimensioned star grains are modeled and solved using the parametric Python script since there are 6 independent response variables. The response variables and their boundaries are listed in Table 8.

Table 8. Response variables and boundaries for star grain.

Variable	Min.	Max.
N	4	6
w, mm	5	15
r_1, mm	5	10
r_2, mm	5	10
ξ, deg	18	28
η, deg	25	40

Percentage effects of the response variables on von Mises stress level of the star grain that is subjected to centrifugal loading are presented in Figure 21.

According to the results, N is the most effective parameter for star grains. Additionally, N, ξ, η, r_1, and w dominates approximately 86% of the results.

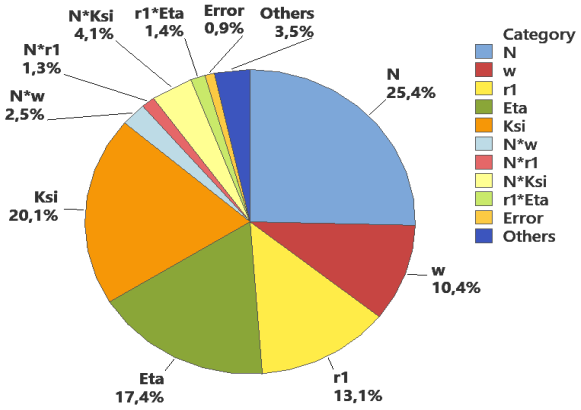

Figure 21. Percentage effects of response variables on von Mises stress results of star grains.

Figure 22 represents the variation of maximum von Mises stress level on the propellant with the variation of N and ξ.

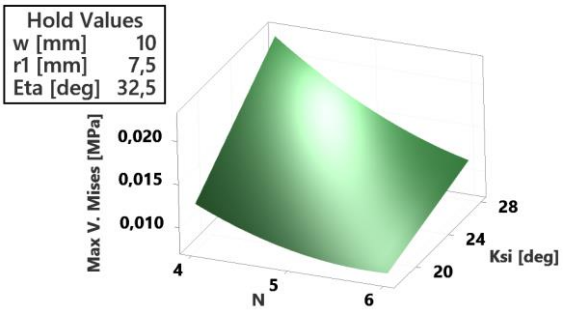

Figure 22. Variation of von Mises stress with N and ξ for star grain.

Figure 23 illustrates the variation of maximum von Mises stress level on the propellant with the variation of N and η.

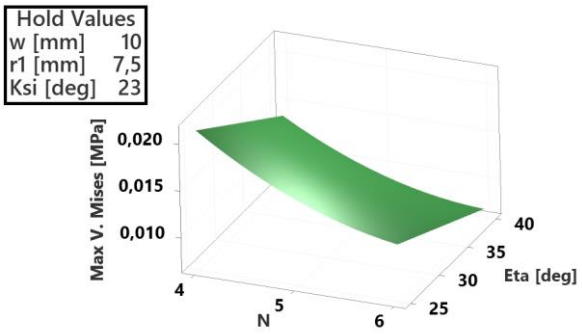

Figure 23. Variation of von Mises stress with N and η for star grain.

Figure 24 shows the variation of maximum von Mises stress level on the propellant with the variation of η and ξ.

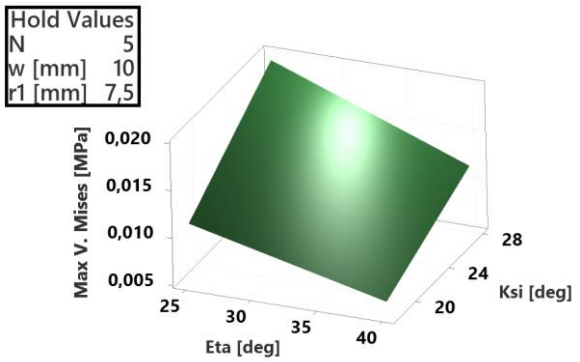

Figure 24. Variation of von Mises stress with η and ξ for star grain.

Figure 25 plots the relationship between maximum von Mises stress level on the propellant with the variation of the response variables.

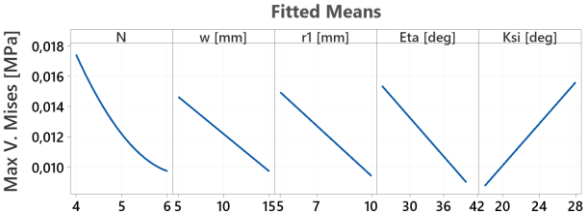

Figure 25. Variation of von Mises stress with response variables for star grain.

Increment of N, w, r_1, η, and a decrement of ξ leads to decrement of the stress level on the propellant. Additionally, there is a nonlinear relationship between N and the stress level while other response variables have a linear relationship with the stress.

5.3. Slotted Grain

To construct the response surface, 25 different finite element models having different dimensioned slotted grains are modeled and solved using the parametric Python script since there are 4 independent response

variables. The response variables and their boundaries are listed in Table 9.

Table 9. Response variables and boundaries for slotted grain.

Variable	Min.	Max.
N	3	5
R_i, mm	15	30
R_p, mm	40	80
f, mm	4	8

Percentage effects of the response variables on von Mises stress level of the slotted grain that is subjected to centrifugal loading are presented in Figure 26.

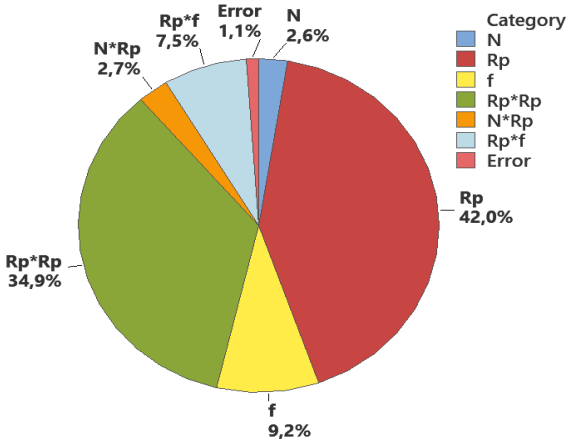

Figure 26. Percentage effects of response variables on von Mises stress results of slotted grains.

According to the results, R_p is the most effective parameter for slotted grains. f parameter has also a considerable effect on maximum stress.

Figure 27 represents the variation of maximum von Mises stress level on the propellant with the variation of R_p and f.

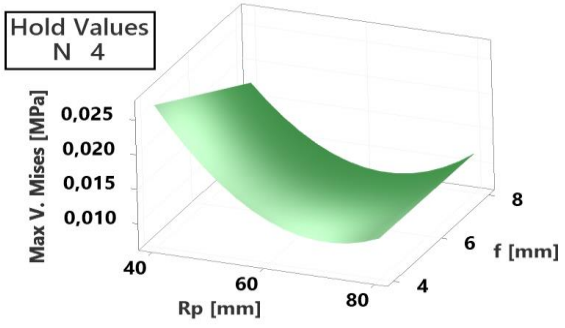

Figure 27. Variation of von Mises stress with R_p and f for slotted grain.

Figure 28 shows the variation of maximum von Mises stress level on the propellant with the variation of N and f.

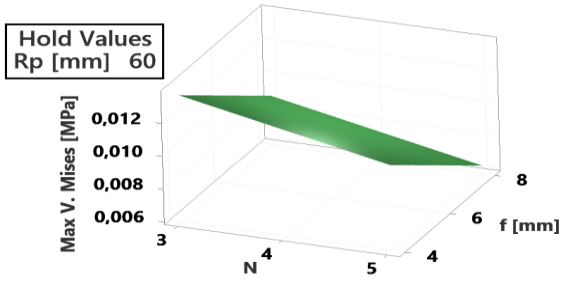

Figure 28. Variation of von Mises stress with N and f for slotted grain.

Figure 29 plots the relationship between maximum von Mises stress level on the propellant with the variation of the response variables.

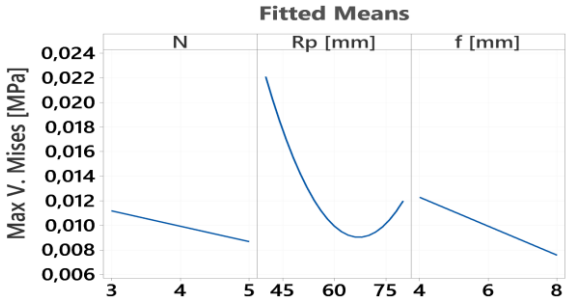

Figure 29. Variation of von Mises stress with response variables for slotted grain.

Increment of N and f leads to a linear decrement of the maximum von Mises stress level on the propellant. On the other hand, there is a nonlinear relationship between R_p and the stress level. An increment of R_p decreases the maximum stress value up to a certain limit.

5.4. Wagon Wheel Grain

To construct the response surface, 145 different finite element models having different dimensioned wagon wheel grains are modeled and solved using the parametric Python script since there are 8 independent response variables. The response variables and their boundaries are listed in Table 10.

Table 10. Response variables and boundaries for wagon wheel grain.

Variable	Min.	Max.
N	4	6
w, mm	5	20
r_1, mm	5	10
r_2, mm	5	10
r_3, mm	5	10
L_a, mm	10	30
ξ, deg	18	28
β, deg	30	40

Percentage effects of the response variables on von Mises stress level of the wagon wheel grain that is

subjected to centrifugal loading are presented in Figure 30.

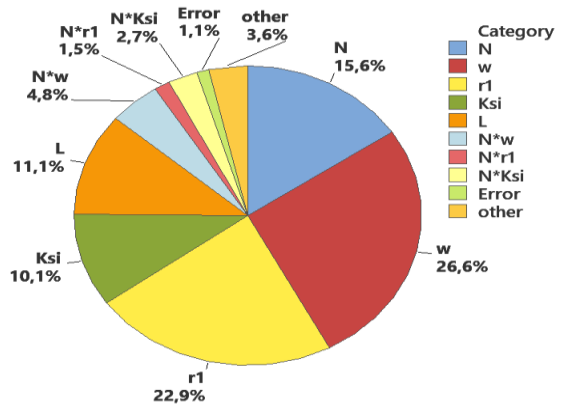

Figure 30. Percentage effects of response variables on von Mises stress results of wagon wheel grains.

According to the results, w is the most effective parameter for wagon wheel grains. Additionally, w, r_1, N, L, and ξ dominates approximately 86% of the results.

Figure 31 shows the variation of maximum von Mises stress level on the propellant with the variation of w and r_1.

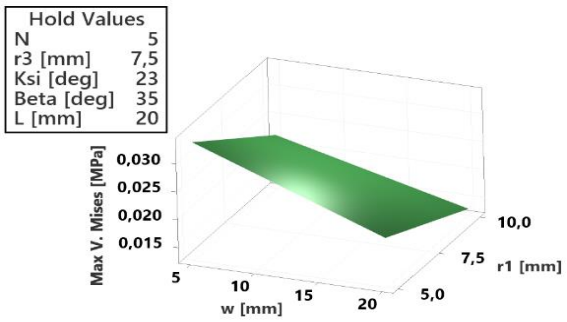

Figure 31. Variation of von Mises stress with w and r_1 for wagon wheel grain.

Figure 32 represents the variation of maximum von Mises stress level on the propellant with the variation of w and N.

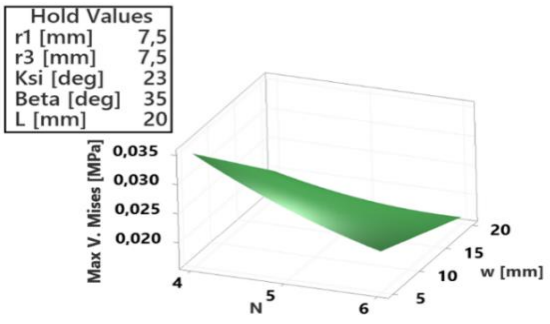

Figure 32. Variation of von Mises stress with w and N for wagon wheel grain.

Figure 33 illustrates the variation of maximum von Mises stress level on the propellant with the variation of r_1 and N.

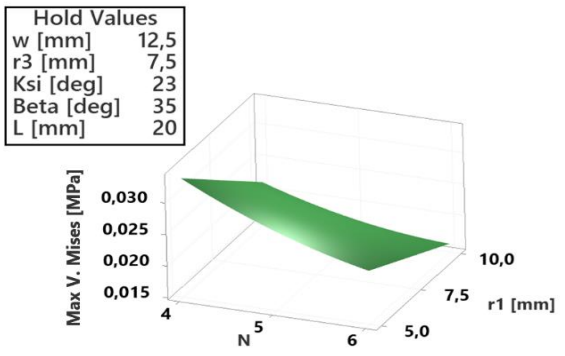

Figure 33. Variation of von Mises stress with r_1 and N for wagon wheel grain.

Figure 34 plots the relationship between maximum von Mises stress level on the propellant with the variation of the response variables.

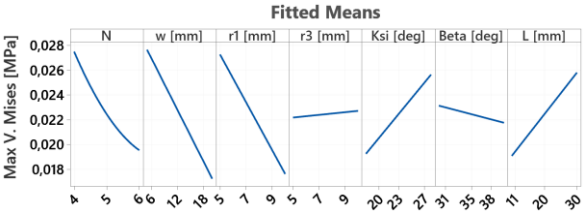

Figure 34. Variation of von Mises stress with response variables for wagon wheel grain.

Increment of N, w, r_1, β and decrement of r_3, ξ, L leads to a decrement of maximum von Mises stress level on the propellant. All response variables are in a linear relationship with the stress level except N.

5.5. Anchor Grain

To construct the response surface, 77 different finite element models having different dimensioned anchor grains are modeled and solved using the parametric Python script since there are 6 independent response variables. The response variables and their boundaries are listed in Table 11.

Table 11. Response variables and boundaries for anchor grain.

Variable	Min.	Max.
N	2	4
w, mm	10	30
L_1, mm	5	15
L_2, mm	5	10
φ, deg	15	30
y_c, mm	20	30

Percentage effects of the response variables on von Mises stress level of the anchor grain that are subjected to centrifugal loading is presented in Figure 35.

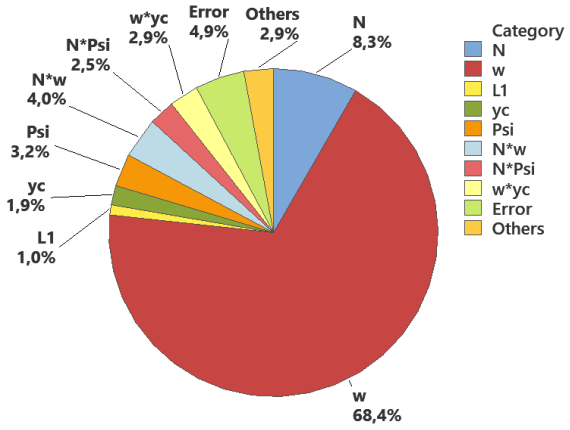

Figure 35. Percentage effects of response variables on von Mises stress results of anchor grains.

According to the results, *w* is the most effective parameter for anchor grains. Additionally, *w*, and *N* dominate approximately 77% of the results.

Figure 36 represents the variation of maximum von Mises stress level on the propellant with the variation of *w* and *N*.

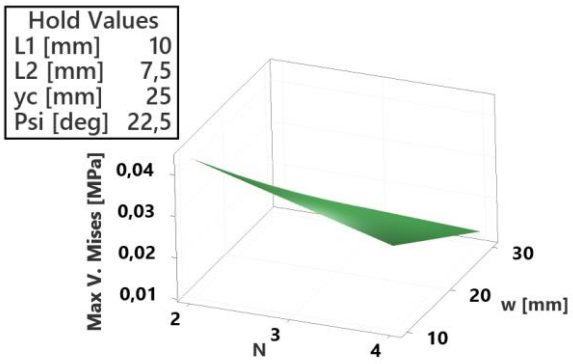

Figure 36. Variation of von Mises stress with *w* and *N* for anchor grain.

Figure 37 plots the relationship between maximum von Mises stress level on the propellant with the variation of the response variables.

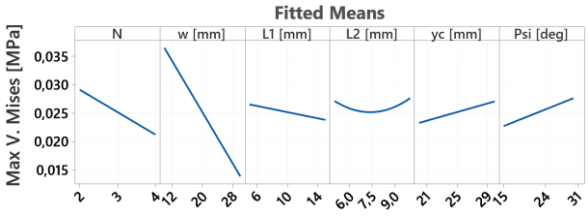

Figure 37. Variation of von Mises stress with response variables for anchor grain.

Increment of *N*, *w*, L_1 and decrement of y_c, φ leads to a decrement in the maximum von Mises stress level on the propellant. On the other hand, L_2 does not have a critical effect on the maximum stress level.

Since the maximum stress is located at sharp edges of the anchor grain, it is possible to decrease the maximum stress level on it by modifying the edges with fillets.

6. CONCLUSION

This work examines the structural behavior of frequently used solid propellants subjected to centrifugal loading that is not previously examined in the literature. Parametric Python scripts are prepared and used to construct and solve the linear viscoelastic finite element models. Finally, response surface analyses are performed and the most effective parameters on von Mises stress level for different grain geometries are determined. Response surface data also represents the type of relationship (such as: linear or nonlinear) between the von Mises stress and the response variables.

Results of this work showed that:

- It is possible to shift the maximum von Mises stress location of a tubular propellant from its inner radius to outer radius by increasing its inner radius value.
- The number of slots (*N*) has a nonlinear relationship with the maximum von Mises stress level of the star, slotted, wagon wheel, and anchor grains.
- *N* is the most effective parameter on the maximum von Mises stress level of the star grains subject to rotational body force.
- R_p parameter dominates the maximum von Mises stress level of the slotted grains.
- *w* is the most effective parameter on the maximum von Mises stress level for both the wagon wheel and the anchor grains subject to rotational body force.
- To decrease the stress level, the propellant volumetric loading fraction should be decreased. This result is valid for all of the examined grain sections since less amount of propellant mass leads to less amount of centrifugal load and so the stress level at the critical location.

7. REFERENCES

[1] Z. Shen, L. Zhang and Y. Li, "Structural integrity analysis and experimental investigation for solid rocket motor grain subjected to low temperature ignition," in *7th Asian Conference on Mechanical and Materials Engineering, MATEC 2019, Tokyo, Japan, June 14-17, 2019.*

[2] N. Gligorijević, S. Antonović, S. Živković, B. Pavković and V. Rodić, "Thermal and acceleration load analysis of new 122 mm rocket," *Scientific Technical Review*, vol. 66, pp. 3-11, December 2016.

[3] K. Qui and X. Zhang, "Finite element analysis of propellant of solid rocket motor during ship

motion," *Propulsion and Power Research*, vol. 2, pp. 50-55, March 2013.

[4] H. Chu and J. Chou, "Effect of cooling load on the safety factor of propellant grains," *Journal of Propulsion and Power*, vol. 29, pp. 27-33, January 2013.

[5] W. M. Adel and L. Guozhu, "Study of Cooldown Thermal Loading Effect on the Bore Deformation of Viscoelastic Solid Propellant Grain," in *AIAA Propulsion and Energy Forum, Atlanta, GA, USA, July 10-12, 2017*.

[6] M. Kurian, K. Renganathan and S. M. Sobichen, "Structural analysis of viscoelastic solid propellant grain," *International Journal of Scientific & Engineering Research*, vol. 7, pp. 117-122, October 2016.

[7] B. Tunç, Ş. Özüpek, E. Podnos and U. Arkun, "Thermal Cyclic Stress Analysis of a Solid Rocket Motor," *Journal of Spacecraft and Rockets*, vol. 56, pp. 179-189, August 2018.

[8] J. D. Mattingly, *Elements of Propulsion: Gas Turbines and Rockets*. American Institute of Aeronautics and Astronautics, Virginia, 2006, pp. 218.

[9] NASA, "Solid Propellant Grain Design and Internal Ballistics," Washington, USA, Tech. Rep. NASA SP-8076, 1972.

[10] C. Tola, and M. Nikbay, "Solid rocket motor propellant optimization with coupled internal ballistic–structural interaction approach," *Journal of Spacecraft and Rockets*, vol. 55, pp. 936-947, April 2018.

[11] C. Tola and M. Nikbay, "Internal ballistic modeling of a solid rocket motor by analytical burnback analysis," *Journal of Spacecraft and Rockets*, vol. 56, pp. 498-516, March 2019.

[12] AGARD, "Structural Assessment of Solid Propellant Grains," Neuilly-Sur-Seine, France, Tech. Rep. AGARD AR-350, 1997.

[13] NASA, "Solid Propellant Grain Structural Analysis," NASA Langley Research Center, Hampton, Virginia, USA, Tech. Rep. NASA SP-8073, 1973.

VITAE

Ceyhun TOLA received his B.Sc. degrees in Aeronautical and Astronautical Engineering Departments from Faculty of Aeronautics and Astronautics, Istanbul Technical University (ITU) under the double major program in 2010. He received his M.Sc. and Ph.D. degrees in Aeronautical and Astronautical Engineering from Institute of Science and Technology, ITU in 2012 and 2017 sequentially. During the M.Sc, he worked as graduate research assistant in ITU Trisonic Lab. During the Ph.D, he worked for Roketsan Missiles Inc., Vestel Defense Industry, and Sun Express Airlines as engineer in between 2011-2016. He worked as assistant professor at Astronautical Engineering Department of University of Turkish Aeronautical Association between 2018-2020. Currently, he has been working for Aselsan Inc. as senior expert engineer since August 2020. His research interests are solid rocket motor design, finite element method, response surface method, aeroelasticity, and design optimization.

Hatice Begüm EYLENOĞLU received her B.Sc. degree in Astronautical Engineering from Faculty of Aeronautics and Astronautics, University of Turkish Aeronautical Association, Turkey in 2020. Her research interests are finite element analysis, structural analysis of solid rocket motors, quadrotor design, and remote operating vehicle design.